CMS: PERFORMANCE, PHYSICS, PERSPECTIVES*

Marcin Konecki

for the CMS Collaboration

Faculty of Physics, University of Warsaw
Hoża 69, 00-681 Warszawa, Poland

(Received April 24, 2014)

During the LHC Run-1 (2010–2013) the CMS experiment received almost 30 fb^{-1} of proton–proton data at the energies of $\sqrt{s} = 7$ and 8 TeV. The accumulated statistics allow CMS to perform frontier measurements at high-energies. In this paper, the CMS detector and its performance are briefly described. The highlights of the CMS results are given. Selected Higgs physics results, measurements of vector boson, top-quark and jets production, $B/B_s \to \mu\mu$ and searches for new phenomena are described. The CMS upgrade plans are presented, including ongoing activities during present accelerator shut-down as well as modifications in the LHC Phase-I and beyond.

DOI:10.5506/APhysPolB.45.1427
PACS numbers: 29.40.–n, 14.80.Bn, 14.40.Nd, 14.70.–e

1. The CMS experiment at the LHC

The Large Hadron Collider (LHC) [1] is an accelerator built at CERN laboratory (European Organization for Nuclear Research) in Geneva, Switzerland. The four main experiments at the LHC produce frontier physics results. In its main mode, the LHC machine is designed to collide protons.

The machine centre-of-mass energy was $\sqrt{s} = 7$ TeV in 2010 and 2011, and $\sqrt{s} = 8$ TeV until the end of 2012, when proton–proton runs in LHC Run-1 ended. It is expected that after restarting in beginning of 2015, the LHC will reach energy of $\sqrt{s} = 13$ TeV, close to the design value of $\sqrt{s} = 14$ TeV.

The Compact Muon Solenoid (CMS) experiment [2] had been successfully operated during LHC Run-1. The collected statistics of about 30 fb^{-1} allowed physicist to perform a variety of measurements and searches, and

* Presented at the Cracow Epiphany Conference on the Physics at the LHC, Kraków, Poland, January 8–10, 2014.

led to the discovery of a Higgs particle [3] (together with the ATLAS experiment [4]) — fundamental to understand the Spontaneous Symmetry Breaking Mechanism and the Standard Model.

The CMS is a general purpose experiment for physics discoveries at the highest luminosities of the LHC. Its central component is a large (6 m diameter and 13 m long) superconductive solenoid. It delivers 3.8 T magnetic field in the inner part of the CMS detector and about 1.8 T inside the iron return yoke.

CMS is traditionally divided into a barrel part (with sub-detectors aligned roughly parallel to the beam pipe) and two endcaps. Next to the beam–beam interaction region, a tracker system is located. It consists of silicon Pixel and silicon Strip Detectors. The CMS tracker provides excellent reconstruction of charged particle tracks and primary and secondary vertices. The tracker is surrounded by an electromagnetic calorimeter (ECAL). It is a homogeneous calorimeter made of lead-tungstate crystals. The energy measurement is supplemented with a sampling brass-scintillator hadron calorimeter (HCAL). The above subdetectors are positioned in the inner part of the CMS detector, inside the solenoid. In the outer part, outside the coil, a muon system is placed. It is dedicated for muon reconstruction and identification. The muon system is based on gaseous detectors: Drift Tubes in the barrel, Cathode Strip Chambers in the endcaps and Resistive Plate Chambers in both barrel and endcaps. The pseudorapidity[1] coverage of CMS depends on a subsystem. The tracking detectors (muon system, tracker) provide reconstruction up to $|\eta| \approx 2.4$–2.5. The calorimeter coverage is enlarged for the purposes of hermeticity and extends up to $|\eta| \approx 3$ in the case of ECAL and $|\eta| \approx 5$ for HCAL.

CMS has two step triggering system designed to reduce 40 MHz LHC input rate down to a few hundreds evens per second suitable for off-line analyses.

The Level-1 Trigger is built using custom-made, partially programmable hardware devices (mostly special-purpose ASICs but also FPGAs where appropriate). It analyses coarsely segmented data from the calorimeter and muon systems only. The Level-1 Trigger selection is based on inclusive single- and multi-object triggers with a threshold relying on estimated (transverse) momenta and energies. It is reducing the event rate below 100 kHz, which is the maximal input rate the CMS High-Level Trigger (HLT) system is capable to handle. HLT is implemented in an expandable computer farm. As of end of LHC Run-1, it consisted of about 13000 CPUs. The executed algorithms use detector data at full granularity, including information from the tracker. They are organised in HLT paths (up to 450) that are seeded

[1] Pseudorapidity $\eta = -\ln \tan \theta/2$, where θ is a polar angle.

by the Level-1 deliverables. The HLT paths are fully customisable. There are paths for delivering inclusive physics objects like leptons or jets and for complicated topologies based on complex algorithms involving: b-tagging, particle isolation, invariant mass computation and other observables.

HLT reduces rate down to 300–500 Hz of "core data" dedicated for a main CMS physics program and, in addition, 300–600 Hz of "parked data" which cannot be promptly reconstructed off-line, for later additional analyses. About 1 kHz of reduced "scouting data", which includes reconstructed objects without raw data suitable for precise analyses, are also stored. In addition, there are dedicated streams for calibration and monitoring.

The CMS on-line and off-line reconstruction algorithms are very similar and differ mainly in calibration methods. The CMS reconstruction includes standard methods based on object reconstruction within a subdetector as well as a Particle-Flow method [5, 6]. The CMS Particle-Flow event reconstruction attempts to identify and reconstruct individually all particles produced in collisions using information from all detectors combined in an optimal way. This method improves performance of reconstructed jets and missing energies as well as identification of leptons and photons. The Particle-Flow method is used in majority of physics analyses in CMS and also at HLT.

The CMS is facing the changing conditions given by the LHC. In 2010 the peak instantaneous luminosity was increased by 5 orders of magnitude, reaching about $2\times10^{32}\,\mathrm{cm}^{-2}\mathrm{s}^{-1}$ at the end of the year. The instantaneous luminosity was further increased to the maximal peak value of $4\times10^{33}\,\mathrm{cm}^{-2}\mathrm{s}^{-1}$ in 2011 and $7.7\times10^{33}\,\mathrm{cm}^{-2}\mathrm{s}^{-1}$ in 2012. The luminosity changes in time are presented in figure 1. The CMS trigger is adapting to running conditions

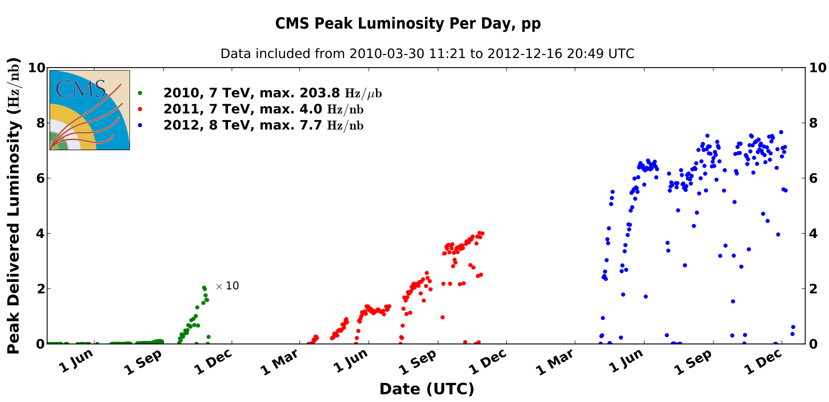

Fig. 1. The evolution of peak instantaneous luminosity in CMS in: 2010 (left part/green, multiplied by a factor of 10), 2011 (middle/red) and 2012 (right/blue). The maximal values in each year are also shown.

by continuous adjustment of trigger menu, defined as a set of executed algorithms. In addition, since the luminosity is also dropping during a single LHC fill, CMS has defined pre-scale factors that can be applied during data taking to keep the CMS Level-1 rate at an optimal level. The luminosity increase affects not only the trigger rates but also a number of overlapping events in one bunch-crossing. At peak luminosity, the event pileup increased from 3.5 in 2010 up to 34.5 in 2012. The average number of pileup events in 2012 reached 21.5 — a value close to the expected pileup for LHC design parameters at $10^{34}\,\mathrm{cm}^{-2}\mathrm{s}^{-1}$ with 25 ns bunch spacing.

In figure 2 the integrated delivered, recorded and validated luminosity is shown. The large pileup and luminosity changes have not compromised the performance of the CMS detector. The efficiency of data taking, given by a ratio of recorded and delivered luminosity varies in the range of 90–93%. The efficiency losses at this point include start–stop run procedure, downtimes due to detector configuration and losses due to limited bandwidth. Improvement of the recording efficiency in 2012 was caused by automatization of run recovery procedures. The recorded CMS data undergo further quality validation procedure. Only validated data are used in the physics

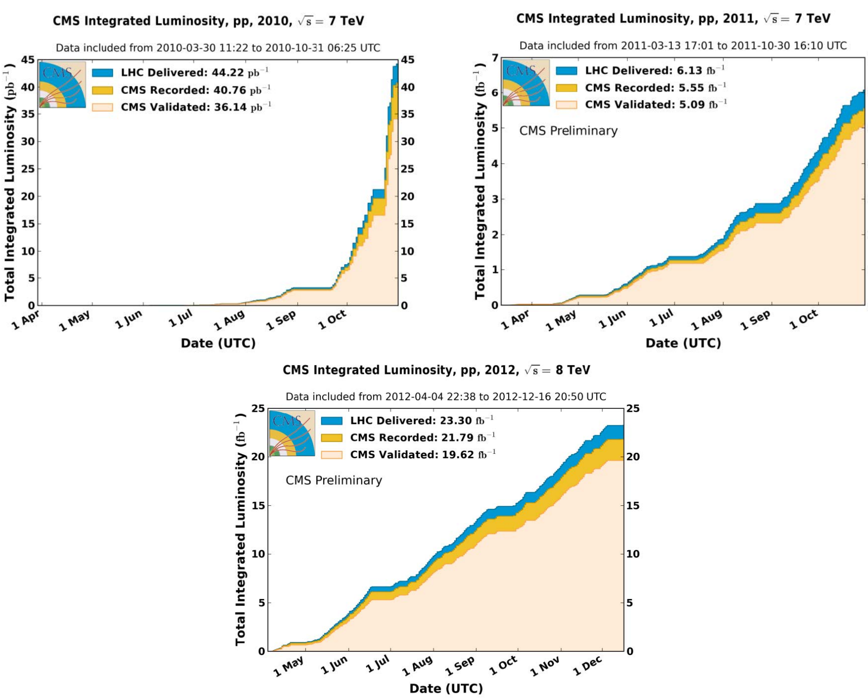

Fig. 2. The delivered, recorded and validated integrated luminosity in 2010 (upper left), 2011 (upper right) and 2012 (bottom). The full statistics of $5.1\,\mathrm{fb}^{-1}$ data at $\sqrt{s} = 7\,\mathrm{TeV}$ and $19.7\,\mathrm{fb}^{-1}$ at 8 TeV is used in the Higgs analysis.

analyses. Approximately 90% of data is validated positively. This fraction is rather constant in time. Among the reasons of qualification of data as bad, there are detector configuration issues, hot or inefficient cells in subdetectors and problems with data processing. CMS also exhibits very good performance in terms of the number of active channels. At the end of LHC Run-1, depending on subdetector, it varied from 96.3% (Pixels) up to 99.9% (HCAL). These fractions of active channels were not visibly degradated since the beginning of CMS operation.

2. Highlights of physics results

The CMS detector was initially commissioned with various test beam data and cosmic runs [7] before start-up of the LHC. Commissioning process was continued with early LHC data. At that time the key aspects were calibration and alignment of subdetectors, validation of reconstruction algorithms, comparison of detector response (reconstructed physics objects) with simulation predictions, validation and tuning of trigger algorithms and menus. The summary of early CMS performance and measurements can be found in Ref. [8]. The rich physics program of the CMS experiment is focused on the Higgs boson. The program also includes searches for New Physics and tests of the Standard Model, including: QCD, electroweak measurements, top-quark physics, b-physics and others. As of begin of 2014 the CMS Collaboration had published 275 physics papers. The summary of most important results is given in following sections.

2.1. The Higgs physics

The origin of the masses of fundamental particles is one of the most exciting questions of Particle Physics. In the Standard Model, particles may acquire masses due to Spontaneous Electroweak Symmetry Breaking, implemented in the Brout–Englert–Higgs mechanism. It predicts an existence of a single scalar boson, called Higgs boson (H). A new boson with a mass around 125 GeV/c, discovered by the ATLAS and CMS collaborations, was identified as the Higgs particle. After the discovery, the theoretical works on the mechanism were honoured by the 2013 Nobel prize in Physics [9]. Currently, the Higgs program of CMS is focused on determination of Higgs boson properties in order to validate compatibility with the Standard Model predictions. Studies include production and decay modes, mass, couplings, and spin-parity measurements.

The main production mechanism of Higgs boson at the LHC energies is via gluon fusion. In this case, since Higgs bosons couple directly to massive objects, it is produced in a virtual top quark loop. The other main production modes are vector boson fusion (VBF) and associated production with vector boson ZH or WH (VH). The VBF Higgs is produced by two W or Z bosons emitted from initial quarks. In this case, Higgs is accompanied by two forward jets resulting from initial quarks. The VH Higgs is radiated by virtual W or Z from initial $q-\bar{q}'$ annihilation. In addition, the Higgs production in association with top quarks (ttH) is also possible. The total Higgs production cross-section for mass around 125 GeV$/c$ is about 20 pb at LHC energies of 7–8 TeV. The main decay modes studied are: $\gamma\gamma$, ZZ, WW, $\tau\tau$ and $b\bar{b}$. The $H\to\gamma\gamma$ and $H\to ZZ\to 4\ell$ (where $\ell=e,\mu$) play a key role due to good significance of the signal and mass resolution. Other processes such as $Z\gamma, \mu\mu$ and ttH are also studied, but current statistics is limited.

The $H\to\gamma\gamma$ is one of the CMS benchmark channels for detector performance and a "golden" channel for low mass Higgs (110 GeV$/c < m_H <$ 150 GeV$/c$) discovery and studies. The perfect di-photon mass resolution and event reconstruction (including photon identification and isolation) allowed CMS to suppress large background and obtain high level of significance despite the fact that the branching fraction of H to $\gamma\gamma$ is of the order of 10^{-3}. The signal signature consists of two high energetic and isolated photons. The background arises from QCD prompt photon production, mis-identification of hadronic jets as photons, or their combination. In the case of hadronic jets mimicking a photon, a neutral meson is often carrying most of the momentum of a jet. Thus it appears to be isolated. A fake photon is formed by collimated photons from a meson decay. In the $H\to\gamma\gamma$ analysis [10], the photons considered must fulfil pre-selection criteria: an electron veto, hadronic leakage and loose selection based on shower shape and isolation. Then, in the analysis baseline, the boosted decision tree (BDT) is used to distinguish between prompt and fake photons. The main constituents for this identification are shower topology and isolation variables. Other objects reconstructed in the event and used in the analysis are: jets, muons, electrons, $E_{\mathrm{T}}^{\mathrm{miss}}$, di-photon vertex. To improve analysis sensitivity the events are grouped into categories related to production mechanisms: di-photon events untagged *i.e.* without tagging objects (gluon fusion), di-photon events with one forward and one backward jet (VBF), di-photon events with high-p_{T} electron, muon or $E_{\mathrm{T}}^{\mathrm{miss}}$ (VH). This untagged and di-jet categories were further subdivided in order to take into account signal sensitivity depending on di-photons kinematics and possible photon conversions. As a result, the 8 TeV data sample was divided into 9 categories. In the case of 7 TeV data, only 5 categories were used.

The analysis exploits multivariate analysis (MVA) techniques. The mass-fit-MVA analysis is done independently in different event classes. These results are weighted by the ratio of signal-to-background in each class and then merged together. The resulting invariant mass distribution is shown in figure 3. A clear peak is visible and a mass of $m_H = 125.4 \pm 0.5(\text{stat.}) \pm 0.6(\text{syst.})$ GeV$/c$ has been fitted to the data. The signal strength modifier obtained in this analysis is $\sigma/\sigma_{\text{SM}} = 0.78 \pm 0.27$ at $m_H = 125$ GeV$/c$. The local significance of 3.2 sigma has been achieved, while 4.2 is expected from the Standard Model. As a cross-check, the cut-based analysis was also performed yielding a local significance of 3.6 sigma (compared to 3.9 expected) and $\sigma/\sigma_{\text{SM}} = 1.11 \pm 0.31$ at $m_H = 124.5$ GeV$/c$. Both analyses are compatible.

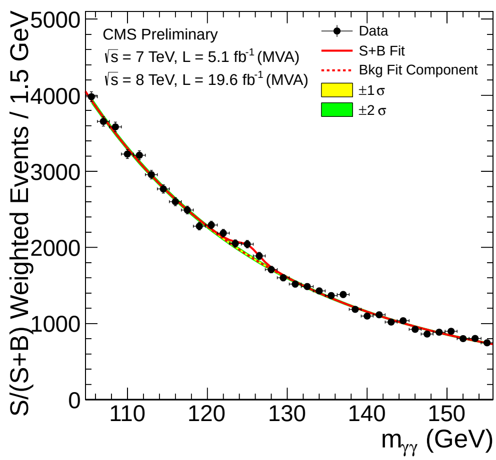

Fig. 3. The invariant mass of selected di-photon events. The histogram entries are weighted according to the event category. The weighting factor is signal over signal and background. Signal and signal with background fit are shown. The 1 and 2 sigma error bands are marked.

The $H \to ZZ \to 4\ell$ channel is another golden channel for detector benchmark and a Higgs discovery channel in wide mass range (110 GeV$/c$ $< m_H <$ 1 TeV$/c$). The signature consists of 2 pairs of opposite charge leptons (e^+e^- or $\mu^+\mu^-$). They must be compatible with ZZ system, where one or both Z may be off-shell. A very small combined branching fraction of the order of 10^{-4} for $m_H = 125$ GeV$/c$ requires optimisation for low-statistic signal. A good mass resolution and high efficiency of lepton identification and reconstruction is mandatory in this search. The clear signature of 4 isolated, high-p_{T} leptons allows to suppress background significantly. The main source of irreducible background is non-resonant ZZ or $Z\gamma^*$ production with their leptonic decays, including tau pairs followed by decays to electron or muons. The remaining small reducible background originates from Z+jets and $t\bar{t}$ pair production.

The $H \to ZZ \to 4\ell$ analysis [11] is based on the reconstruction of electrons and muons. It requires efficient identification, good momentum reconstruction and optimised isolation methods. The electron reconstruction and identification incorporates information from the ECAL and tracker subdetectors. It is relying on a multivariate discriminant, which takes into account possible bremsstrahlung, matching between tracker and ECAL and shower-shape. The muon reconstruction algorithm combines observables from the tracker and muon system. The resulting muon candidate is a combination of reconstructed tracks in both system. Low-p_{T} tracks cannot fully penetrate muon detectors and in this case a muon is identified by track in the tracker matched to observables from one or two muon stations. The muon track identification also includes compatibility with small deposit in the calorimeters. The lepton reconstruction can be improved by correcting for final-state radiation (FSR). The FSR photons are mostly collinear with direction of their parent lepton. Another key aspect of the analysis is lepton isolation. It is based on a sum of momenta of tracks within an isolation cone around the lepton, relative to the lepton momentum. All four leptons and the tracks used for isolation must be compatible with a primary vertex identified by a sum of p_{T}^2 of all associated tracks. The analysis is supplemented with jet measurements used for the event classification in order to separate VBF/VH and gluon fusion Higgs production mechanisms.

The analysis uses matrix element likelihood approach (MELA) framework [3]. The $4e$, 4μ and $2e2\mu$ sub-channels are analysed separately due to different background and mass resolution. Apart of four-lepton invariant mass, the kinematic discriminant based on leptons angular distribution and di-lepton pairs invariant masses improves signal sensitivity and reduces statistical uncertainty of the results. The jet information and combined p_{T} of a 4-lepton system provide additional discriminant for production mechanism.

In figure 4 the distribution of the invariant mass is shown for events passing selection criteria. The expected background and signal peak for $m_H = 126$ GeV/c are indicated. The signal and background are extracted from a fit to the invariant mass and other observables. The mass of the Higgs boson is determined to be $m_H = 125.6 \pm 0.4(\mathrm{stat.}) \pm 0.2(\mathrm{syst.})$ GeV/c. The signal strength modifier obtained from this analysis is $\sigma/\sigma_{\mathrm{SM}} = 0.93^{+0.26}_{-0.23}(\mathrm{stat.})\,^{+0.13}_{-0.09}(\mathrm{syst.})$. This channel confirms existence of the Higgs boson with a local significance of 6.8 standard deviations.

The CMS Collaboration has independent analyses for all main Higgs decay modes. Besides of $\gamma\gamma$ and ZZ decay channels described above, decays to WW [12], $b\bar{b}$ [13] and $\tau\tau$ [14] are also studied. The results were combined [15] in order to better determine properties of the newly discovered boson and to validate compatibility with the Standard Model.

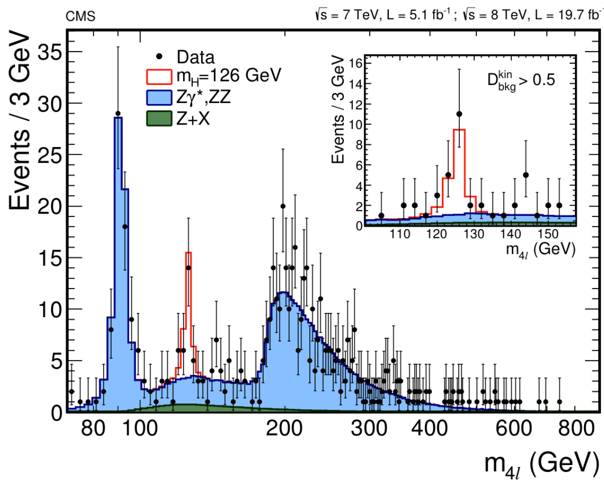

Fig. 4. The invariant mass distribution of selected 4 lepton events. The main expected backgrounds from ZZ and $Z\gamma^*$ are indicated. The expected signal is marked as a red (empty) histogram.

The summaries of production cross-section and couplings are shown in figure 5. The sub-channels of CMS analyses were classified according to tagged production mechanism and then combined. The resulting cross-section for Higgs boson production relative to the Standard Model prediction is $\sigma/\sigma_{\rm SM} = 0.8 \pm 0.14$. It is in agreement with the Standard Model. The measured cross-section for particular production mechanisms and decay modes (not shown here) are also consistent with the Standard Model predictions [15].

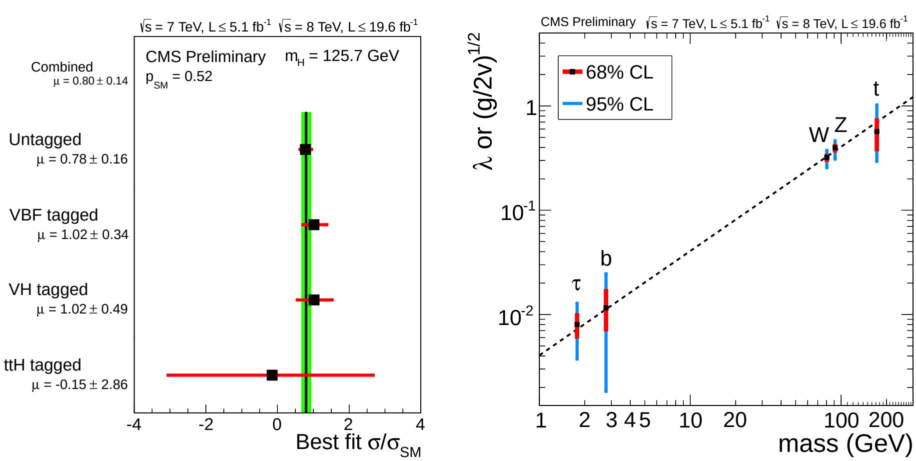

Fig. 5. Signal strength modifier for tagged Higgs production mechanisms (left) and the Higgs couplings dependence on the particle mass (right).

Another important test performed by the CMS is a study of spin and parity of the Higgs boson, see figure 6. The analyses [15–17] rely on angular distributions of leptons and photons. The results favour $J^{\mathrm{P}} = 0^+$ hypothesis which is consistent with the Standard Model prediction.

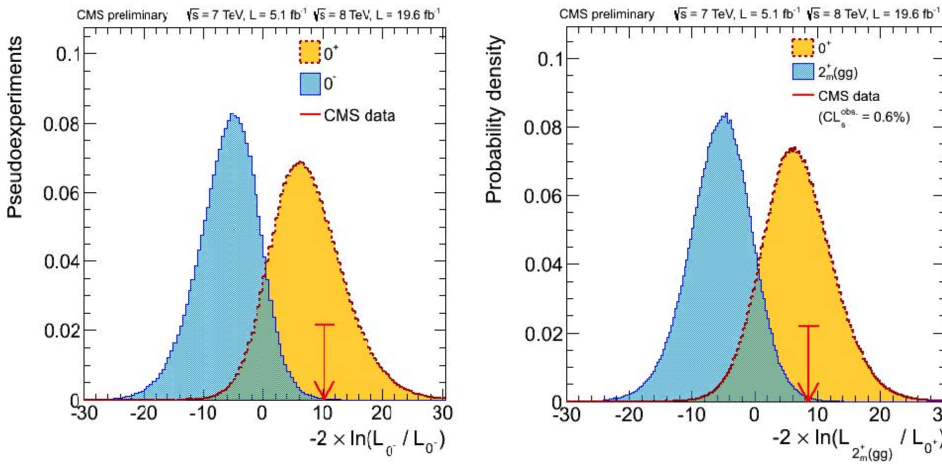

Fig. 6. Higgs Spin-Parity tests. The distributions of test statistic comparing 0^+ hypothesis and $2^+_m(gg)$ — graviton-like boson with minimal couplings produced in gluon fusion (right, ZZ and WW data) and 0^- (left, ZZ data). The CMS measurements, in favour of 0^+ state, are marked with arrows.

2.2. Vector boson production, top measurements and QCD

The precision measurements of electroweak processes provide: tests of the Standard Model, constraints for parton distribution functions and tools for detector calibration. A good understanding of W and Z measurements is necessary for Higgs and New Physics searches since the vector bosons are involved in decay chains and may be sources of background for discoveries.

The CMS Collaboration has measured inclusive cross-section for W and Z production soon after the LHC startup at 7 TeV [18] followed by associated production with jets. The measurements at 8 TeV [19] uses data from a dedicated low pile-up run. With more statistics in hand the di-boson production cross-section was also measured in: $W\gamma, Z\gamma, WW, WZ$ and ZZ channels. The obtained results are in perfect agreement with theoretical predictions.

The studies of di-boson and tri-boson production provide important test of the electroweak sector of the Standard Model. The CMS found [20] no evidence for the ZZZ and $ZZ\gamma$ couplings which are forbidden in the Standard Model. Also no evidence has been found for anomalous quartic gauge couplings in the studies of three boson production with $W\gamma(Z/W)$ [21], nor in WW study probing $WW\gamma\gamma$ coupling [22]. The limits for anomalous couplings were set.

The dedicated analysis of hadronic activity in Z accompanied by 2 jets events [23] allowed the CMS to establish $2.6\,\sigma$ evidence for the Vector Boson Fusion contribution to the Z production. This measurement is important in the context of: Higgs VBF production, electroweak gauge couplings and vector-boson scattering.

The top quark production measurements are another important point of the CMS physics program as these are essential elements of the Standard Model calculations, constraining the Higgs mass. The existence of the top quark was confirmed by the CMS experiment soon after the LHC start-up. The measurements include production cross-sections and mass determination. The analysis of the $t\bar{t}$ pair production cross-section at $\sqrt{s} = 8\,\mathrm{TeV}$ in the most accurate di-lepton channel yields $\sigma_{t\bar{t}} = 239 \pm 2(\mathrm{stat.}) \pm 11(\mathrm{syst.}) \pm 6(\mathrm{lumi.})\,\mathrm{pb}$ [24]. The corresponding result at 7 TeV is $\sigma_t\bar{t} = 162 \pm 2(\mathrm{stat.}) \pm 5(\mathrm{syst.}) \pm 4(\mathrm{lumi.})\,\mathrm{pb}$ [25]. The combined top mass is $m_{\mathrm{top}} = 173.49 \pm 0.36(\mathrm{stat.}) \pm 0.91(\mathrm{syst.})$ GeV$/c$ [26]. The combination includes measurements from di-lepton method, lepton and jets, all-jets, kinematic end-points and a recently used b-hadron lifetime.

Additional top quark studies include: cross-section for the single top production in a t-channel [27], the associated tW production [28], the $t\bar{t}$ charge asymmetry [29], and the top quark polarization in the single-top production in a t-channel [30].

The measurements of differential inclusive jet production cross-section provide an important test of the perturbative QCD theory. The CMS measurement [31] extends to jet transverse energies above 2 TeV in perfect agreement with NLO calculations over 10 orders of magnitude. The jet production measurements constraint proton–parton distribution functions and provide measurements of the strong coupling constant at a TeV scale. The CMS determines α_{s} using several analyses, based on: the inclusive jet cross-section [32], the ratio of 3-jet to 2-jet production [33], the measurement of the 3-jet mass cross-section [34], and the measurement of the $t\bar{t}$ production cross-section [35].

2.3. A search for rare $B/B_s \to \mu^+\mu^-$ decays

The $B/B_s \to \mu^+\mu^-$ decays have been extensively studied for many years as they may be sensitive to New Physics. The B and B_s decays to $\mu^+\mu^-$ pairs are rare in the Standard Model as the flavour changing neutral currents are forbidden at a tree level. The decay involves higher-level, penguin and box diagrams. The predicted branching fraction is $(3.23 \pm 0.27) \times 10^{-9}$ for

B_s and $(1.07 \pm 0.10) \times 10^{-10}$ for B decays to $\mu^+\mu^-$ [36]. These branching fractions may be substantially modified by supersymmetric models and other extensions to the Standard Model.

CMS has measured [37] a branching fraction of $\mathrm{BR}(B_s \to \mu^+\mu^-)$ to be $(3.0^{+1.0}_{-0.9}) \times 10^{-9}$ with a significance of $4.3\,\sigma$ ($4.8\,\sigma$ expected). The upper limit on $\mathrm{BR}(B \to \mu^+\mu^-)$ was set to 1.1×10^{-9}.

The analysis is based on a search for di-muon events with an invariant mass around a signal region of $m_{\mu\mu}$ of 5.2–5.45 GeV$/c$. The combinatorial background for di-muons from different B-meson decays is estimated by extrapolation from outside B–B_s mass range. The additional background from b-hadronic or semi-muonic decays, convoluted with possible particle misidentification as a muon, is taken from simulation. The different mass resolution and background level for the barrel- and endcap-part of detector as well as the different LHC energy is taken into account by dividing the data into categories. The data is further binned depending on the output of BDT, trained to distinguish between signal and background events.

An unbinned likelihood fit is used to extract the signal and background yields. The fit combines B and B_s candidate events with the expected background. The illustrative combination of weighted categories and the corresponding significance is shown in figure 7.

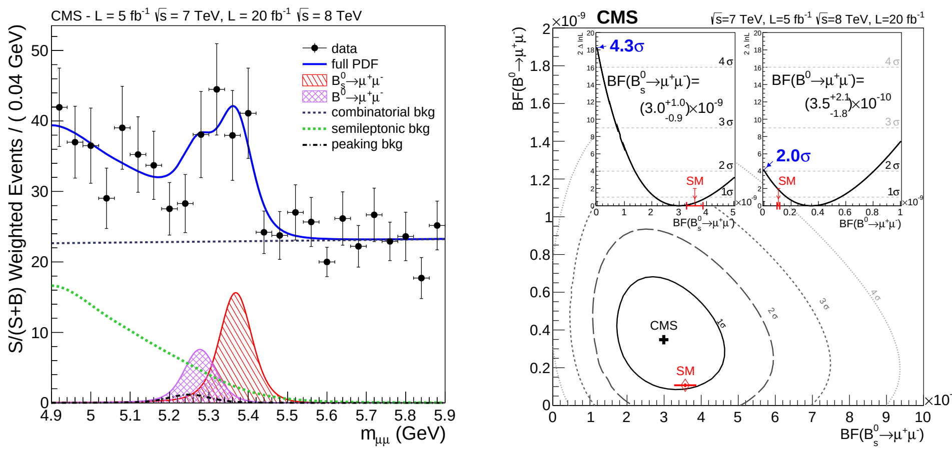

Fig. 7. Left: Plot illustrating the combination of all categories used, combined by weight depending on signal and background levels. Right: Scan of the ratio of the joint likelihood for branching ratios of $B_s \to \mu^+\mu^-$ and $B \to \mu^+\mu^-$ with the profiled likelihood distributions for B_s and B separately shown as insets. The grey/red points show standard model expectations.

In the analysis, the $B^{\pm} \to J/\psi K^{\pm}$ channel with J/Ψ muonic decays is used to normalise branching fraction in order to reduce uncertainties on the $b\bar{b}$ production cross-section and the luminosity. The $B_s \to J/\Psi\Phi \to \mu^+\mu^-K^+K^-$ channel is used as a control sample.

The combined CMS and LHCb measurement [38] is $\mathrm{BR}(B_s \to \mu^+\mu^-) = (2.9 \pm 0.7) \times 10^9$.

2.4. Searches for a new phenomena beyond the Standard Model

The Standard Model, with the recent discovery of the Higgs boson, is confirmed to be a successful theory. However, it does not cope with astrophysics measurements: does not provide candidates for Dark Matter, nor explains sizable matter–antimatter asymmetry. Thus searches for the New Physics, not predicted by the Standard Model are important and intriguing part of the CMS physics program.

There is a large number of theories providing large spectra of new phenomena beyond the Standard Model, but the supersymmetry (SUSY) is often meant to be a natural extension of the Standard Model. In the R-parity conserving models the lightest SUSY particle is a candidate for Dark Matter. Since it may escape undetected from the detector the search strategy includes large unbalanced energies. Another important observables in the search for new phenomena are leptons and multiple jets. The CMS is currently focused on inclusive analyses. Simplified models are used to provide interpretation of results in terms of limits for masses of supersymmeteric objects. The limits are model dependent. The gluino exclusion limit reaches masses up to 1.4 TeV/c, while for other particles ranges the exclusion limits are often well below 1 TeV/c. A wide range of results and limits is available at [39].

CMS exotica tests [40] include search for heavy gauge bosons (W', Z'), long-lived particles, Randall–Sundrum gravitons, leptoquarks, compositness, excited fermions, Large Extra Dimensions and Dark Matter. Within a variety of states, the typical signatures of interest are: high-momentum dileptons, di-jets, di-bosons, events with large missing energy and single jets or photons, high multiplicity and multi-jet events.

Currently, the searches of New Physics in CMS show no significant deviation from the Standard Model predictions in any of the search channels.

3. CMS upgrades during LHC Phase-I and later

The LHC Run-1 has ended in the beginning of 2013 and the LHC entered Long Shutdown I (LS1). During the period of LS1, the LHC is improving the magnet interconnections. These improvements and the dipole magnet training program will allow the LHC to provide proton–proton collisions at the energy $\sqrt{s} = 13$ TeV, close to the design LHC parameters. The beginning of a next data taking, is expected to take place in 2015. Several luminosity scenarios are possible, among them the option with 25 ns bunch spacing and the instantaneous luminosity of $1.6 \times 10^{34}\,\mathrm{cm}^{-2}\mathrm{s}^{-1}$ and the event pile-up about 50. In the next shut-down, LS2 (2018–2020) the upgrade of the LHC injector is planned what will further increase the instantaneous luminosity up to $2 \times 10^{34}\,\mathrm{cm}^{-2}\mathrm{s}^{-1}$. The Phase-I LHC will be finished around 2022, with a planned accumulated integrated luminosity of over $300\,\mathrm{fb}^{-1}$. The Phase-II, after LS3 (planned for 2023–2025), will further increase luminosity to target integrated luminosity of $3000\,\mathrm{fb}^{-1}$. The modernizations of the LHC machine will be accompanied by necessary upgrades [41] of the CMS apparatus to deal with more difficult experimental conditions, radiation, detector ageing, but also to improve the detector performance.

In the ongoing LS1, the important modification in the detector geometry is the upscope of muon system. This will provide additional, 4$^{\mathrm{th}}$ muon station in endcaps, equipped with RPC and CSC detectors. It is especially important for the RPC based sub-trigger which is currently working with limited efficiency. The additional measurement will also further constraint muon trajectory patterns, improving Level-1 triggering.

Increasing accelerator energy and luminosity impose high purity triggering already at Level-1. Otherwise, to keep the Level-1 rate within a design bandwidth of 100 kHz, a substantial increase of trigger thresholds is required, affecting physics performance. To improve purity, the Level-1 system will be rebuilt with a modern electronics [42], to enable more advanced algorithm executions. The calorimeter trigger modifications goals are: improved electromagnetic object isolation and pile-up subtraction, jet finding and hadronic tau identification. On the muon side, the transverse momentum resolution should be improved. The Global Level-1 trigger will allow for a more sophisticated relations between objects involved in the algorithm and for more trigger algorithms available in the trigger menu. The possibility to use calorimeter based data for muon isolation is considered.

The muon trigger will undergo major logic changes. Currently, the trigger response is generated independently by muon sub-triggers: (RPC PACT trigger, DT Track Finder and CSC Track Finder) and trigger candidates are combined by a Global Muon Trigger. Within the new Muon Track Finder, the underlying detector signals will be delivered to one data processing unit and the resulting muon candidate will take into account all the available information. It is especially important in the barrel-endcap transition region where number of measurements is limited. Since the detector layout is changing with pseudorapidity, the system will be partitioned into barrel-, overlap- and endcap-part, enabling different algorithm optimisation depending on the detector region. The preparation to the Level-1 trigger upgrade requires modifications of detector electronics, including important changes to data transmission electronics. It is an ongoing activity.

The triggering is a vital aspect of an experiment and the CMS experiment cannot put data on risk. Hence, after LS1 a part of detector data will be split and delivered both to legacy and a new system. The new system will thus coexist with the current one for commissioning purposes during data taking. The full replacement is targeted for the winter shut-down 2015/16.

Several modernisations of the hadronic calorimeter are planned during LHC Phase-I [43]. The ability to reject an anomalous background rate will be increased and depth segmentation will be improved. The forward calorimeter signal readout uses conventional, single-channel Photo-Multipliers tubes (PMTs) to collect light from fibers. To reduce system sensitivity to anomalous signals caused by particle passing through photo-tubes the multi-anode PMTs will be used instead. In the hadronic outer (HO), barrel (HB) and endcap (HE) calorimeters, the signal readout is done with Hybrid Photodiode transducers (HPDs), where uncontrolled electrical discharges appear. The effect is particularly stubborn in the HO. The HPDs will be replaced with Silicon Photo-Multipliers (SiPM). The forward calorimeter (HF) and HO modifications are assigned to LS1, while HB and HE, which are less affected by readout problems are scheduled for LS2. The use of new SiPM modules enables finer granularity (segmentation in 3 depths in barrel and 5 in endcaps). The readout electronics will also be replaced, TDC capability will be included and a new data link technology will be used. The above changes will allow better tracking of hadronic shower in the CMS reconstruction.

The replacement of the CMS Pixel Detector is another major CMS upgrade project [44]. The main motivations for it, is the performance degradation which current detector will suffer with luminosity increase. The current pixel readout chip (ROC) has limited buffer size and readout speed. For a target luminosity of $1 \times 10^{34}\,\mathrm{cm}^{-2}\mathrm{s}^{-1}$ with an average pileup of about 25, it will introduce a readout inefficiencies of about 4% in the first pixel layer for 25 ns bunch spacing. The higher pileup due to luminosity increases and possible 50 ns bunch structure may dramatically worsen the readout inefficiencies up to 50% for a first layer in a luminosity scenario of $2\times10^{34}\,\mathrm{cm}^{-2}\mathrm{s}^{-1}$ with 50 ns bunch spacing. In addition, the current detector radiation hardness is not sufficient for a long operation at luminosities exceeding design LHC parameters.

Therefore, a new Pixel Detector is designed. The new readout chip, based on the current one but with improved buffer depths, readout speed and readout technique will be used. A low level efficiency losses are obtained from simulations. For the most inner layer, a loss of 2.4% is predicted for conditions of $2 \times 10^{34}\,\mathrm{cm}^{-2}\mathrm{s}^{-1}$ with 25 ns bunch spacing. The new Pixel Detector, compared to present one, is shown in figure 8. It is optimised to provide 4 measurements up to $|\eta| < 2.5$. In the barrel part, it will consist of 4 layers and 3 disks in each endcap. The higher number of measurements points will not only improve tracking and vertexing precision but enables more precise and cleaner seeding with efficient pixel hit triplets. It is crucial for triggering at high luminosity.

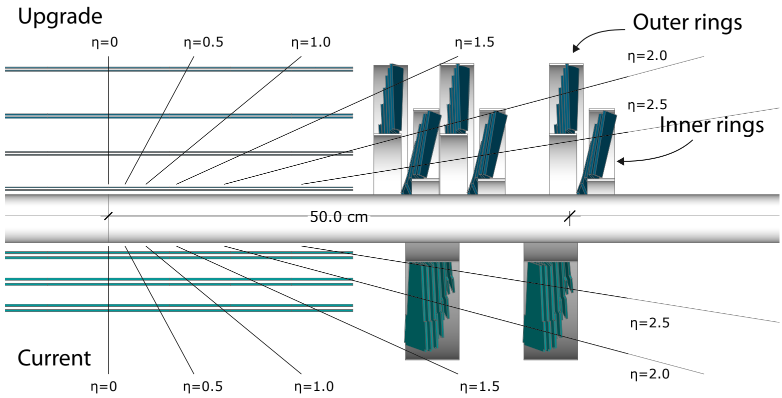

Fig. 8. The current (bottom part of the plot) and upgraded (upper part) CMS Pixel detector. The new barrel layers will be located at radii: 2.9, 6.8, 10.2 and 16.0 cm and the new endcap disks at $|z|$: 29.1, 39.6 and 51.6 cm.

The low-material budget of tracking devices, that are surrounded by calorimeter system, is mandatory. Although an additional pixel layer is added, the movement of readout electronics and connectors further-out, and a new cooling system reduced the amount of passive material. The new powering scheme will be deployed.

In order to facilitate the Pixel Detector exchange, a beam-pipe with a smaller diameter (45 mm) is installed during LS1. The replacement of detector is foreseen in winter stop 2016/17, which will be extended to 6 months to enable this operation.

A further detector upgrades are needed due to luminosity increase at LHC Phase-II. The studies for the detector modifications, including simulations, and intensive R&D, are ongoing. The CMS Collaboration is targeting for a Phase-II upgrade technical proposal in 2014.

The modifications necessary for Phase-II will include further changes to tracking, muon and calorimeter systems, both pixel and strip tracker will be replaced. To sustain a luminosity increase by a factor of 5 with respect to design, accompanied by large radiation level the new strips in tracker will have increased granularity. The new outer tracker will be formed by 6 barrel layers and 5 endcap disks. The number of pixel disks may be further extended to cover the pseudorapidity up to about 4. The outer part of a new tracker will also have triggering capabilities, supported by joined sensors

(p_{T}-modules) able to locally discriminate between high- and low-p_{T} tracks. The Level-1 tracks with p_{T} about a certain threshold (typically $2\,\mathrm{GeV}/c$) may be formed at the back-end.

The extended coverage of a tracker and its triggering capabilities will be supplemented with modification of a muon system. The currently limited, coverage of the RPC subsystem may be completed up to pseudorapidity about 2.4 with GEM detectors and Glass-RPC, providing additional signals for muon triggering. At higher angles, the usage of additional muon detectors to possibly tag a track as a muon is under discussion.

Significant changes are also expected in forward calorimeters, where usage of more radiation tolerant photo-detectors and new scintillation material is mandatory. The Phase-II LHC will also induce important changes to Level-1, HLT, and DAQ systems.

4. Summary

The CMS detector had been operated successfully during LHC Run-1. The good efficiency of operation and good overall performance of the apparatus resulted in the $5.1\,\mathrm{fb}^{-1}$ data at $\sqrt{s} = 7\,\mathrm{TeV}$ and $19.7\,\mathrm{fb}^{-1}$ at $8\,\mathrm{TeV}$ used in CMS analyses. The discovery of a new boson, identified as the Higgs boson, is the most important CMS discovery so far. The mass of the Higgs boson measured in $\gamma\gamma$ channel is $m_H = 125.4 \pm 0.5(\mathrm{stat.}) \pm 0.6(\mathrm{syst.})\ \mathrm{GeV}/c$ and in four lepton channel $m_H = 125.6 \pm 0.4(\mathrm{stat.}) \pm 0.2(\mathrm{syst.})\ \mathrm{GeV}/c$. The other Higgs boson decay channels were studied as well. The combined signal strength modifier parameter for the Higgs boson is 0.8 ± 0.14. The analysis of the Higgs boson properties also confirms couplings and spin-parity values as predicted by the Standard Model. The CMS Collaboration has a rich program of precise measurements and tests of the Standard Model, including W, Z, top quark, and jet measurements. The current results do not show any deviations from the Standard Model predictions. The CMS has measured branching fraction of $B_s \to \mu^+\mu^-$ decay and set a limit on $B \to \mu^+\mu^-$. The wide range of searches for signs of supersymmetry and other exotic models has been performed and no signals of physics beyond the Standard Model have been found so far. The CMS detector preparation for LHC Run-2 is ongoing. The Phase-I upgrades of hadronic calorimeter, silicon and muon sub-detectors and trigger are underway, in particular preparations for major modifications of the Level-1 trigger concept and installation of new, better pixel detector. In parallel, the upgrades for LHC Phase-II are under study.

REFERENCES

[1] L. Evans, Ph. Bryant (editors), *JINST* **3**, S08001 (2008).
[2] CMS Collaboration, *JINST* **3**, S08004 (2008).
[3] CMS Collaboration, *Phys. Lett.* **B716**, 30 (2012).
[4] ATLAS Collaboration, *Phys. Lett.* **B716**, 1 (2012).
[5] CMS Collaboration, technical report CMS-PAS-PFT-09-001, CERN, 2009.
[6] CMS Collaboration, `arXiv:1401.8155 [hep-ex]`.
[7] CMS Collaboration, *JINST* **5**, T03001 (2010).
[8] CMS Collaboration, *Acta Phys. Pol. B* **42**, 1443 (2011).
[9] The Nobel Prize in Physics 2013, `Nobelprize.org`, Nobel Media AB 2013, `http://www.nobelprize.org/nobel_prizes/physics/laureates/2013/`
[10] CMS Collaboration, technical report CMS-PAS-HIG-13-001, CERN, Geneva, 2013.
[11] CMS Collaboration, `arXiv:1312.5353 [hep-ex]`.
[12] CMS Collaboration, *J. High Energy Phys.* **1301**, 096 (2013) [`arXiv:1312.1129 [hep-ex]`].
[13] CMS Collaboration, *Phys. Rev.* **D89**, 012003 (2014) [`arXiv:1310.3687 [hep-ex]`].
[14] CMS Collaboration, `arXiv:1401.5041 [hep-ex]`.
[15] CMS Collaboration, technical report CMS-PAS-HIG-13-005, CERN, Geneva, 2013.
[16] CMS Collaboration, technical report CMS-PAS-HIG-13-016, CERN, Geneva, 2013.
[17] CMS Collaboration, *Phys. Rev. Lett.* **110**, 081803 (2013) [`arXiv:1212.6639 [hep-ex]`].
[18] CMS Collaboration, *J. High Energy Phys.* **1110**, 132 (2011) [`arXiv:1107.4789 [hep-ex]`].
[19] CMS Collaboration, technical report CMS-PAS-SMP-12-011, CERN, Geneva, 2012.
[20] CMS Collaboration, technical report CMS-PAS-SMP-13-005, CERN, Geneva, 2013.
[21] CMS Collaboration, technical report CMS-PAS-SMP-13-009, CERN, Geneva, 2013.
[22] CMS Collaboration, *J. High Energy Phys.* **1307**, 116 (2013) [`arXiv:1305.5596 [hep-ex]`].
[23] CMS Collaboration, *J. High Energy Phys.* **1310**, 062 (2013) [`arXiv:1305.7389 [hep-ex]`].
[24] CMS Collaboration, *J. High Energy Phys.* **1402**, 024 (2014) [`arXiv:1312.7582 [hep-ex]`].

[25] CMS Collaboration, *J. High Energy Phys.* **11**, 067 (2012) [arXiv:1208.2671 [hep-ex]].

[26] CMS Collaboration, technical report CMS-PAS-TOP-13-002, CERN, Geneva, 2013.

[27] CMS Collaboration, arXiv:1403.7366 [hep-ex].

[28] CMS Collaboration, technical report CMS-PAS-TOP-12-040, CERN, Geneva, 2013.

[29] CMS Collaboration, technical report CMS-PAS-TOP-12-033, CERN, Geneva, 2013.

[30] CMS Collaboration, technical report CMS-PAS-TOP-13-001, CERN, Geneva, 2013.

[31] CMS Collaboration, technical report CMS-PAS-SMP-12-012, CERN, Geneva, 2013.

[32] CMS Collaboration, technical report CMS-PAS-SMP-12-028, CERN, Geneva, 2013.

[33] CMS Collaboration, *Eur. Phys. J.* **C73**, 2604 (2013) [arXiv:1304.7498 [hep-ex]].

[34] CMS Collaboration, technical report CMS-PAS-SMP-12-027, CERN, Geneva, 2013.

[35] CMS Collaboration, *Phys. Lett.* **B728**, 496 (2013) [arXiv:1307.1907 [hep-ex]].

[36] A.J. Buras, J. Girrbach, D. Guadagnoli, G. Isidori, *Eur. Phys. J.* **C72**, 2172 (2012) [arXiv:1208.0934 [hep-ph]].

[37] CMS Collaboration, *Phys. Rev. Lett.* **111**, 101804 (2013).

[38] CMS and LHCb collaborations, technical report CMS-PAS-BPH-13-007, CERN-LHCb-CONF-2013-012, CERN, Geneva, Jul. 2013.

[39] CMS Supersymmetry Physics Results, https://twiki.cern.ch/twiki/bin/view/CMSPublic/PhysicsResultsSUS

[40] CMS Exotica Public Physics Results, https://twiki.cern.ch/twiki/bin/view/CMSPublic/PhysicsResultsEXO

[41] CMS Collaboration, technical report CERN-LHCC-2011-006, LHCC-P-004, CERN, Geneva, Jun. 2011.

[42] CMS Collaboration, technical report CERN-LHCC-2013-011, CMS-TDR-12, CERN, Geneva, Jun. 2013.

[43] CMS Collaboration, technical report CERN-LHCC-2012-015, CMS-TDR-10, CERN, Geneva, Sep. 2012.

[44] CMS Collaboration, technical report CERN-LHCC-2012-016, CMS-TDR-11, CERN, Geneva, Sep. 2012.